Unipolar-pulse amplitude modulation frequency division multiplexing for visible light communication systems

Osama Saied,[a,*] Zabih Ghassemlooy,[b] Stanislav Zvanovec,[c] Refik Caglar Kizilirmak,[d] and Bangjiang Lin[e]

[a]University of Gharyan, Department of Electrical and Electronic Engineering, Gharyan, Libya
[b]Northumbria University, Optical Communications Research Group, Faculty of Engineering and Environment, United Kingdom
[c]Czech Technical University in Prague, Department of Electromagnetic Field, Prague, Czech Republic
[d]Nazarbayev University, Department of Electrical and Computer Engineering, Astana, Kazakhstan
[e]Chinese Academy of Sciences, Quanzhou Institute of Equipment Manufacturing, Haixi Institutes, Quanzhou, China

Abstract. Asymmetrically clipped optical orthogonal frequency division multiplexing (ACO-OFDM) has been proposed in visible light communication (VLC) systems to overcome the dc-biased optical OFDM power consumption issue at the cost of the available electrical spectral efficiency. Due to the implementation of inverse fast Fourier transform, all the optical OFDM schemes including ACO-OFDM suffer from large peak-to-average power ratio (PAPR), which degrades the performance in VLC systems as the light-emitting diodes used as the transmitter have a limited optical power-current linear range. To address the PAPR issue in ACO-OFDM, we introduce a unipolar-pulse amplitude modulation frequency division multiplexing by adopting the single carrier frequency division multiple access (SC-FDMA). This is achieved by considering a PAM as an SC-FDMA data symbol and inserting a conjugate copy of the middle and first SC-FDMA FFT output subcarriers after the middle and last subcarriers, respectively. Simulation results show that, for the proposed scheme, the PAPR is 3.6 dB lower compared with ACO-OFDM. The PAPR improvement is further analyzed with the simulation results demonstrating that the proposed scheme offers 2.5 dB more average transmitted power compared to ACO-OFDM. [DOI: 10.1117/1.OE.59.9.096108]

Keywords: single carrier frequency division multiple access; asymmetrically clipped optical orthogonal frequency division multiplexing; visible light communication; peak-to-average power ratio; light-emitting diode; dynamic range.

Paper 20200745 received Jun. 23, 2020; accepted for publication Sep. 10, 2020; published online Sep. 29, 2020.

1 Introduction

Visible light communications (VLC) is a wireless technology that uses light-emitting diode (LED)-based sources for the dual purpose of lighting and data communications.[1,2] Unlike radio frequency (rf)-based systems, the light spectrum is unregulated, and VLC can use the entire spectrum or portions of the visible spectrum (385 to 790 THz).[1,2] Nevertheless, the transmission bandwidth in VLC systems is mostly limited by the modulation bandwidth of the LED B_{mod}. For example, the bandwidth of the standard high-power white phosphor LED, which is used for illumination, is in the range of a few MHz.[1,2]

To address the LED's bandwidth limitation, and therefore, increase the transmission data rates, a few methods have been proposed in the literature. For example, the multiple-input

*Address all correspondence to Osama Saied, E-mail: osama.dhawi.saied@hotmail.com

0091-3286/2020/$28.00

multiple-output (MIMO) technique, where higher capacity and diversity gain can be achieved using spatial multiplexing and repetition coding as compared with single-input single-output systems.[3] MIMO has also been used together with multicarrier transmission as in Refs. 4 and 5, where the link capacity was improved using adaptive transmission in frequency selective channels. In addition, in Ref. 6, optical blue filtering was applied at the Receiver (Rx) to suppress the slow response of the phosphor, whereas the analog pre- and postequalization techniques were investigated in Refs. 7–9 to increase B_{mod} and consequently improve the VLC throughput. For instance, in Ref. 7, B_{mod} of the blue, red, and green LEDs with the emitter degenerated LED driver was increased by (i) 106, 87, and 98 MHz, respectively, using a pre-equalizer; and (ii) 174, 180, and 145 MHz, respectively, based on the pre- and postequalizers. However, the improvement in B_{mod} was achieved at the cost of reduced signal-to-noise ratio (SNR) per transmitted symbol at the Rx.[10,11]

Alternatively, to improve B_{mod}, a nonorthogonal multiple access method was considered for multiple access channels,[12,13] where all the user terminals share the entire available bandwidth at the same time. In addition to the aforementioned techniques, multilevel modulation signal schemes including M-ary pulse amplitude modulation have also been demonstrated to increase the data rate.[14] However, instead of single carrier modulation (SCM), a multicarrier modulation schemes such as orthogonal frequency division multiplexing (OFDM) have been adopted to boost the transmission data rate in VLC systems. For instance, in a recent demonstration,[15] the data rate of more than 15 Gbps was reported using OFDM with optimum bit and power loading based on wavelength division multiplexing of four LEDs (i.e., RGBY). Although OFDM has many promising benefits in VLC, traditional OFDM signal generation techniques used in rf systems cannot be directly applied to intensity modulation and direct detection (IM/DD)-based VLC systems. First and foremost, in IM/DD systems, the information bearing signal should be non-negative and real valued. In the literature, the three most commonly used optical OFDM techniques are dc-biased optical OFDM (dcO-OFDM), asymmetrically clipped optical OFDM (ACO-OFDM), and pulse amplitude modulated discrete multitone (PAM-DMT), all of which rely on Hermitian symmetry (HS) in the complex symbol vector prior to time-domain signal generation through inverse fast Fourier transform (IFFT). HS ensures that, the signal at the output of IFFT is real valued. In order to satisfy the non-negativity condition, dcO-OFDM systems add a dc bias before clipping the negative residual signal, whereas the even subcarriers (SCs) of ACO-OFDM and the real part of PAM-DMT data symbols are kept blank so that the negative amplitudes levels at the output IFFT of both schemes convey no information and hence are clipped. As compared with rf systems, in IM/DD-based OFDM VLC transmission, the electrical spectral efficiency is halved for dcO-OFDM while it is reduced to one-fourth in ACO-OFDM and PAM-DMT. However, ACO-OFDM and PAM-DMT are more optical power efficient and have lower noise clipping compared with dcO-OFDM.[16–20] Due to inclusion of a number of SC components during the IFFT operation, OFDM waveforms suffer from high peak-to-average power ratio (PAPR). This leads to several practical issues, which need addressing such as the limited dynamic ranges of digital-to-analog converter (DAC) and electrical amplifiers, but particularly in VLC systems, the limited linear dynamic range of LED's optical power-current characteristics, which can lead to reduced PAPR, and therefore, distortions of the transmitted and received signals.[21,22] In order to avoid high PAPR, instead of OFDM, single-carrier frequency division multiple access (SC-FDMA) was proposed in Refs. 23–25. SC-FDMA has two types: localization frequency division multiple access and interleaved frequency division multiple access (IFDMA), and is currently employed for the uplink multiple access schemes in the long-term evolution of cellular systems by the third-generation partnership project.[26,27] ACO-single carrier frequency-domain equalization (ACO-SCFDE) was proposed in Refs. 23 and 24 as a modified IFDMA scheme, which is suitable for IM/DD. The only difference between ACO-OFDM and ACO-SCFDE is the inclusion of FFT and IFFT blocks in the ACO-SCFDE transmitter (Tx) and ACO-SCFDE Rx, respectively. However, to meet IM/DD requirements, the IFDMA symbol vector in all these modified schemes again needs to satisfy HS, which results in increased PAPR in optical-based IFDMA compared with rf-based IFDMA. In Ref. 25, it was demonstrated that because of HS, only half of the ACO-SCFDE samples would have a single carrier PAPR behavior, while the other half will have the same PAPR as in OFDM. However, in our recent work,[28,29] we showed that the PAPR of optical IFDMA can be improved by not

considering the HS requirement and therefore making it as low as the PAPR of IFDMA in the rf domain. This was achieved in Ref. 29 by symmetrically repeating the IFDMA time-domain symbol twice by means of setting the interleaving factor (Q) in the frequency domain to be 2. That is, the IFDMA symbol was transmitted through two subsymbols, where the real and imaginary parts of IFDMA time domain samples were transmitted using the first and second subsymbols, respectively. However, for VLC systems, the first SC (i.e., the dc term) is used for keeping the LED on, dimming or shifting the amplitude levels within the dynamic range of LEDs.[1,2] Because of the implementation of the interleaving mapping and FFT process at the Tx, the first SC in Refs. 28 and 29 needs to be a modulated SC, which is affected by the dc bias and consequently affects all samples in the time domain, resulting in 2 dB of SNR penalty compared with traditional optical OFDM to achieve the same bit error rate (BER) as demonstrated in Ref. 29.

In this paper, the unipolar-PAM frequency division multiplexing (U-PAM-FDM) signaling scheme for the IM/DD-based VLC system is introduced as a means to improve the PAPR of the optical OFDM. This improvement is achieved by removing the requirement for HS in IFDMA and without any dc bias effects. Here, since we have adopted PAM as the data symbols (i.e., real values), the FFT SCs outputs at the IFDMA Tx are symmetrically conjugated except for the first and the middle SCs. However, to make all SCs symmetrically conjugated, two additional SCs are included after the middle and the end of the FFT output, which we call it the symmetrically conjugate (SCG) process. Implementing odd modulation and IFFT on theses modified SCs results in a real and asymmetric signal suitable for IM/DD-based VLC systems.

The paper is structured as follows; Sec. 2 presents the proposed U-PAM-FDM scheme. Results obtained for the proposed scheme are analyzed and evaluated in Sec. 3. Finally, conclusions are drawn in Sec. 4.

2 U-PAM-FDM System Description

In this section, we outline the details of the Tx and the Rx for U-PAM-FDM.

2.1 *U-PAM-FDM Tx*

Figure 1 shows the block diagram of the U-PAM-FDM Tx. An input random serial binary bit stream bi is first converted into the parallel bit streams prior to being mapped to PAM. The generated output signal $C = \{C_0, C_1, C_2, C_3 \ldots\ldots C_{D-1}\}$, where D is the number of transmitted data symbols, which is a real vector, is applied to the FFT module with the output given as

$$S_m = \sum_{d=0}^{M-1} c_d e^{\frac{-j2\pi dm}{M}}, \tag{1}$$

where $S = \{S_0, S_1, S_2, \ldots\ldots S_{M-1}\}$, M is the FFT size, which is equal to D, and m and d are the m'th SC and d'th data symbols, respectively.

Since C is a real signal (i.e., PAM), all SCs at the output of FFT are symmetrically conjugated around the $S_{(\frac{M}{2}+1)}$ SC except the S_0, see Fig. 2. Note, the m'th SC is given as

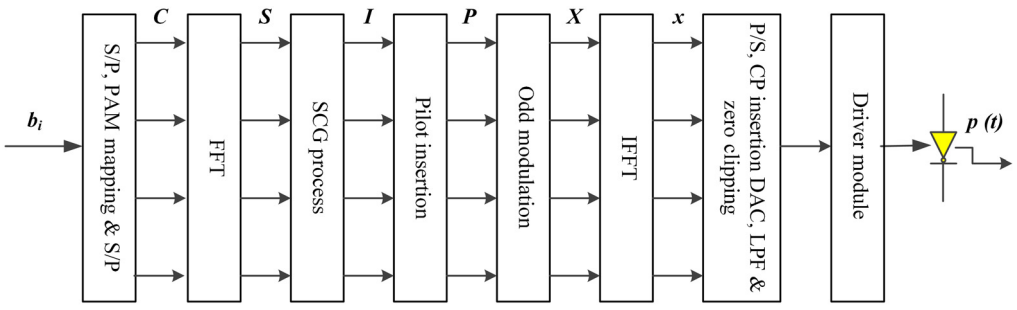

Fig. 1 The block diagram of the U-PAM-FDM Tx.

Fig. 2 The SCs for eight real input samples at the output of the FFT module.

$$\begin{aligned} S_m &= \sum_{d=0}^{M-1} C_d e^{-j2\pi dm/M}, \\ S_{M-m} &= \sum_{d=0}^{M-1} C_d e^{-j(2\pi dm/M)(M-m)}, \\ &= \sum_{d=0}^{M-1} C_d e^{-j[2\pi m-(2\pi dm/M)]}, \\ &= \sum_{d=0}^{M-1} C_d e^{j(2\pi dm/M)}. \end{aligned} \tag{2}$$

From Eq. (2) and Fig. 2, it can be clearly observed that each m'th SC is conjugated with the $(M-m)$'th SC (i.e., $S_m = S^*_{M-m}$), since C is composed of real values. However, to obtain an asymmetric real-time domain signal, which is the requirement for IM/DD VLC links, all the SCs must be symmetrically conjugated (i.e., $S_m = S^*_{M-m+1}$) by then to apply to the SCG block, where two additional SCs [i.e., $S^*_{(\frac{M}{2}+1)} = S^*_4$ for $M = 8$ and S^*_0] are included to S after the center and the last SCs. The SCG output vector, which is shown in Fig. 3, is given as

$$I = \{I_0, I_1, I_2, I_3, \ldots\ldots I_{Z-1}\}, \quad I = \left\{S_0, S_1, \ldots, S_{\frac{M}{2}}, S_{(\frac{M}{2}+1)}, S^*_{(\frac{M}{2}+1)}, S^*_{\frac{M}{2}}, \ldots S^*_1, S^*_0\right\}, \tag{3}$$

where $Z = M + 2$.

For the purpose of channel estimation, a number of SCG pilots are inserted to I as shown in Fig. 4 and is given as

$$P = \{P_0, P_1, P_2, P_3, \ldots\ldots P_{V-1}\}, \tag{4}$$

where $V = Z + A$ and A is the number of pilots, which depends on the channel characterization. P is subsequently applied to the odd modulation and IFFT modules, the outputs of which are given by, respectively,

$$\begin{aligned} X &= \{X_0, X_1, X_2 \ldots\ldots, X_{T-1}\}, \\ &= \{0, P_0, 0, P_1, 0, P_2 \ldots\ldots, 0, P_{Z-1}\}, \end{aligned} \tag{5}$$

$$x_n = \frac{1}{N}\sum_{k=0}^{N-1} X_k e^{\frac{2\pi nk}{N}}, \tag{6}$$

where $T = 2V$, N is the IFFT points, and n and k are the n'th time-domain samples of x and the k'th frequency-domain SC of X, respectively. Note that the output of the IFFT is now a real

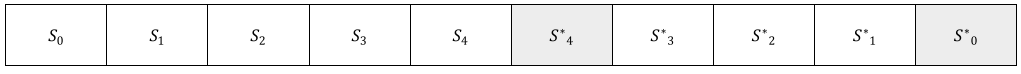

Fig. 3 The frequency-domain SCs at the output of the SCG module for $M = 8$ and $Z = 10$.

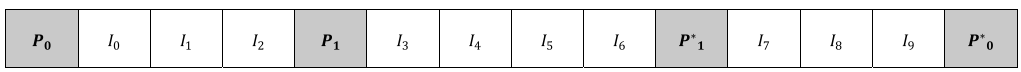

Fig. 4 The frequency-domain SCs with pilot signals for $Z = 10$ and $A = 4$.

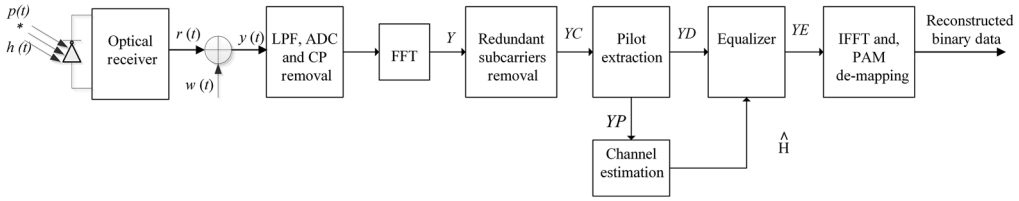

Fig. 5 The block diagram of the U-PAM-FDM Rx.

asymmetric signal. Finally, as in the traditional ACO-OFDM scheme, x is applied to the parallel to serial (P/S), a cyclic prefix (CP), DAC, low pass filter (LPF), and zero clipping module prior to IM of the LED via the driver unit.

2.2 *U-PAM-FDM Rx*

Figure 5 shows the schematic block diagram of the U-PAM-FDM Rx. Following optical detection, the received signal is given as

$$y(t) = r(t) + w(t), \tag{7}$$

where the regenerated electrical signal $r(t) = Rp(t) * h(t)$, R is the responsivity of the photodetector (PD), which is assumed to be unity in this work, $p(t)$ is the transmitted optical signal, symbol $*$ denotes the linear convolution, $h(t)$ is the impulse response of the system, and $w(t)$ represents the shot (signal and ambient light) and terminal noise sources, which are modeled as the additive white Gaussian noise. $y(t)$ is then passed through the LPF, ADC, and CP removal modules prior to being converted to the frequency domain Y using the FFT. Subsequently, the redundant SCs (i.e., the even SCs) are removed from Y and the resulting signal YC is applied to the pilot extraction block to recover the pilot symbols (YP) for channel estimation. The received random data symbols YD together with the estimated transfer function of the system $\hat{H}$ are applied to a single-tab zero forcing equalizer with the output given as

$$YE = \frac{YD}{\hat{H}}. \tag{8}$$

Finally, YE is applied to the IFFT and PAM demapping blocks to generate the estimated data stream.

3 Results and Analysis

In this section, the simulation results for the performance of the U-PAM-FDM scheme are presented. We consider 256 IFFT points and a CP with a duration of 50 ns, which is the maximum time delay for the multipath indoor VLC channel.[30] A 1-W white LED with printed circuit board (PCB) (HPB8-49KxWDx) is used with a 1-V quasilinear dynamic range where its measured L–I–V curve is shown in Fig. 6.

To obtain an optimum comparison among U-PAM-FDM, ACO-OFDM, and ACO-SCFDE in terms of the SNR, BER, and error vector magnitude (EVM), the PAM symbols of U-PAM-FDM are generated at the Tx by separating the real and the imaginary parts of quadrature amplitude modulation (QAM) symbols [i.e., the $(a + bj)$ QAM symbol is separated into 'a' and 'b' PAM symbols], where these symbols are combined together at the Rx to reconstruct the QAM. All the key parameters adopted for simulation are given in Table 1.

The probability of the PAPR being higher than a certain threshold level (i.e., PAPR_0) is shown in Figs. 7 and 8 where, as in Refs. 32–34, a complementary cumulative distribution function (CCDF) of 10^{-4}, i.e., $Pr\{\text{PAPR} > \text{PAPR}_0\} = 0.0001$, is considered.

Figure 7 shows the CCDF as a function of the PAPR for the ACO-OFDM, ACO-SCFDE, and U-PAM-FDM schemes where ACO-OFDM has higher PAPR values by ~3.6 and ~2.1 dB compared with U-PAM-FDM and ACO-SCFDE, respectively. The PAPR improvement of the

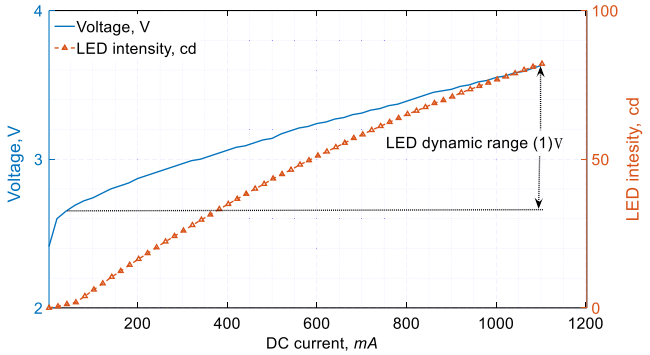

Fig. 6 Measured *L–I–V* curves of the 1-W white LED (HPB8-49KxWDx) (Northumbria University Research Lab).

Table 1 Key simulation parameters.

Parameter	Value
Number of iterations	1 M
LED type	1 W white LED with PCB (HPB849KxWDx)
LED bandwidth	2 MHz
LED linearity	~1 V
The distance between LED and PD	2 m
LED half-power angle $\varnothing_{1/2}$	70 deg
PD	Thorlab (PDA36A-EC)[31]
PD gain	0 dB
PD bandwidth	10 MHz
PD noise (rms)	300 μV
PD responsivity	0.65 A/W
PD active area	16 mm^2
Rx field of view (FOV)	180 deg

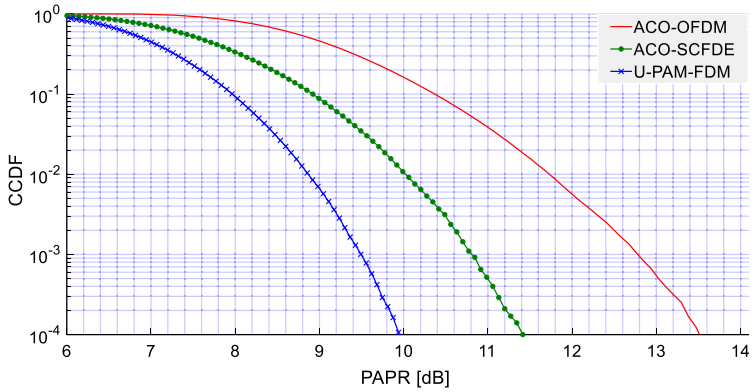

Fig. 7 CCDF versus PAPR for ACO-OFDM, ACO-SCFDE, and U-PAM-FDM.

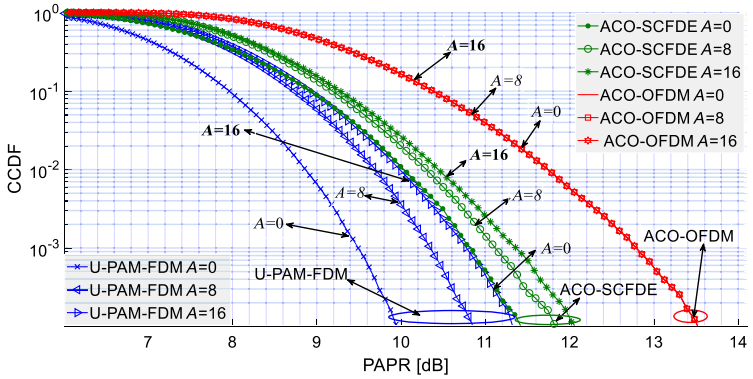

Fig. 8 CCDF versus PAPR for ACO-OFDM, ACO-SCFDE, and U-PAM-FDM with and without the pilot symbols where A is the number of pilots.

ACO-SCFDE and U-PAM-FDM schemes is due to the insertion of the FFT and the interleaving mapping (i.e., odd modulation) blocks prior to IFFT at the OFDM Tx. Note by doing so, OFDM PAPR is as low as the SCM scheme reported in Ref. 27. However, in IM/DD ACO-SCFDE and U-PAM-FDM VLC systems, the HS and SCG blocks should be implemented following FFT at the Tx, which leads to increased PAPR compared with the SCM scheme, since not all SCs enjoy the mapping feature.

Next, we investigated the effect of pilot insertion on the PAPR for ACO-OFDM, ACO-SCFDE, and U-PAM-FDM and compared them with no pilot cases, as shown in Fig. 8. The plots shown clearly demonstrate that at CCDF of 10^{-4}, ACO-SCFDE and U-PAM-FDM with eight pilots (i.e., $A = 8$, where A is the number of pilots) have higher PAPRs by 0.4 and 0.9 dB, respectively, compared with the cases with no pilot symbols. For $A = 16$ for ACO-SCFDE and U-PAM-FDM, the increase in PAPRs is 0.6 and 1.3 dB, respectively, where the insertion of the pilots has no impact on the ACO-OFDM PAPR. These increases of the PAPR for ACO-SCFDE and U-PAM-FDM are due to the insertion of pilot symbols, which change the order of the SCs, thus reducing the number of SCs benefiting from the mapping feature. However, the insertion of pilots may not be required in VLC systems, since the indoor channel is highly stable and deterministic, which can be estimated once and then adopted for the incoming symbols.

Finally, the impact of PAPR on the performance of VLC is numerically investigated by considering the limited LED power-current dynamic range, as was discussed earlier. Since the OFDM schemes have different PAPR values, their transmit average electrical powers (P_{avg}) reach the maximum value of the LED dynamic linear range (L_{D_Max}), i.e., clipping level at different dBm values, which can be obtained from the EVM.

Figure 9 shows the EVM as a function of P_{avg} for the 16- and 256-QAM ACO-OFDM, ACO-SCFDE, and U-PAM-FDM schemes for the average noise power σ_n^2 of -10 dBm. As shown in Fig. 9, the EVM reduces by increasing P_{avg}, reaching the minimum level (i.e. reaching L_{D_Max})

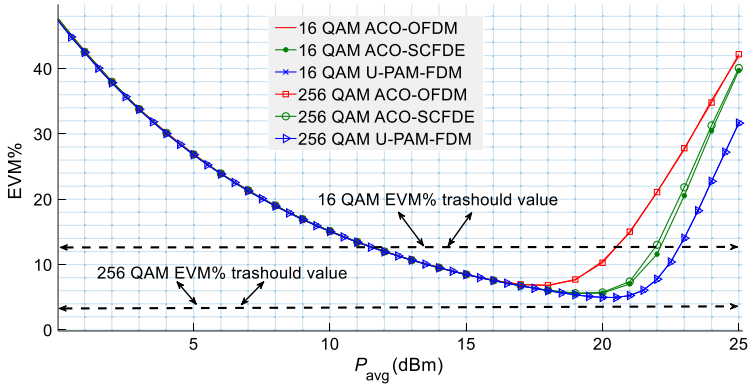

Fig. 9 EVM versus P_{avg} for 16- and 256-QAM ACO-OFDM, ACO-SCFDE, and U-PAM-FDM.

at $18 < P_{\text{avg}} < 21$ dBm depending on the OFDM schemes where the best EVM performance is achieved for U-PAM-FDM as it has the lowest PAPR value. However, after these P_{avg} values, the EVM starts increasing as the system performance starts to be affected by the clipping noise where the maximum achievable average electrical power is obtained when EVM reaches its threshold values.

According to Refs. 35 and 36 for 16- and 256-QAM, the EVM threshold values should be ≤12.5% and 3.5%, respectively. As such for 16-QAM, U-PAM-FDM provides 2.5- and 1-dB higher P_{avg} than ACO-ODM and ACO-SCFDE schemes, respectively. However, for 256 QAM, none of these schemes reach the EVM threshold level as they require a wider LED dynamic linear range (i.e., >1 V). Note that increasing the order of QAM for the same scheme has no impact on the L_{D_Max}.

Next, we investigate the effect of the clipping noise on the BER performance as a function of P_{avg} for 16-, 64- 128-, and 256-QAM ACO-OFDM, ACO-SCFDE, and U-PAM-FDM and for σ_n^2 of −10 dBm, as shown in Fig. 10. These plots illustrate that the proposed scheme outperforms ACO-OFDM and ACO-SCFDE for all QAM constellation orders because of the lowest PAPR value. Figure 10(a) shows that, although ACO-OFDM has a higher PAPR value compared with ACO-SCFDE, it outperforms ACO-SCFDE at lower order QAM signals (i.e., ≤16-QAM), This is because ACO-OFDM distributed time-domain samples provide lower clipping noise, which can be reduced at the Rx using soft and hard decision methods when a lower QAM is considered.

However, for higher order QAM signals, even the low clipping noise cannot be treated at the Rx, and therefore, for >16 QAM constellation order, the scheme with the lower PAPR will provide an improved BER performance as can be easily observed from Fig. 10(b) where the U-PAM-FDM scheme provides the best BER performance, while ACO-OFDM has the worst one.

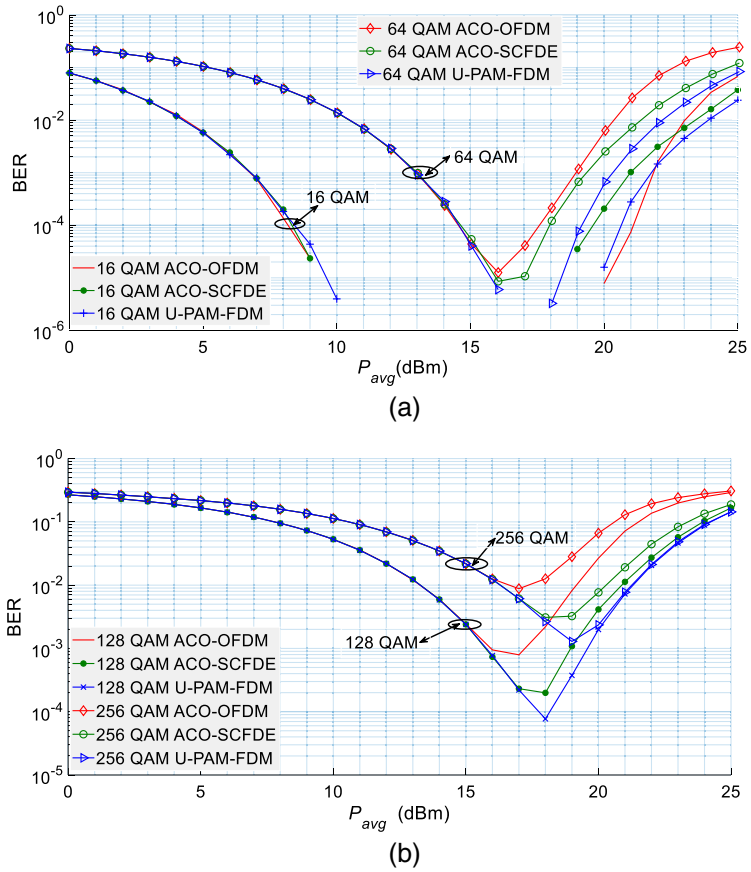

Fig. 10 The BER as a function of P_{avg} for ACO-OFDM, SCFDE, and UPAM-FDM with: (a) 16- and 64-QAM and (b) 128- and 256-QAM.

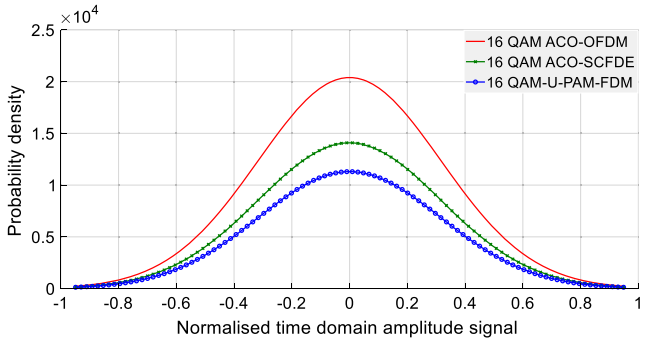

Fig. 11 Normal distribution function for ACO-OFDM, ACO-SCFDE, and U-PAM-FDM data symbols.

Finally, Fig. 11 shows the distribution of 100 k time-domain samples of ACO-OFDM, ACO-SCFDE, and U-PAM-FDM. From the figure, one can observe that most of the ACO-OFDM time-domain samples are distributed around the mean value (i.e., zero value), where the number of samples with large amplitudes for ACO-OFDM is low compared with the other two schemes, which results in a lower number of clipped samples (i.e., lower clipping noise). This explains why ACO-OFDM outperforms ACO-SCFDE for lower QAM constellation orders (i.e., $\leq$16-QAM) as was shown in Fig. 10(a). Note that although the time-domain samples of U-PAM-FDM and ACO-SCFDE have almost the same distribution, U-PAM-FDM outperforms ACO-OFDM for all QAM constellation orders because of its lowest PAPR value as was already discussed.

4 Conclusion

We introduced a new unipolar PAM-FDM scheme to reduce PAPR of unipolar optical OFDM by modifying SC-FDMA for used in IM/DD-based VLC. For U-PAM-FDM, the simulation results showed that the PAPR values are 3.6 and 1.5 dB lower compared with ACO-OFDM and ACO-SCFDE, respectively. We also investigated the impact of reducing PAPR on the EVM performance and showed that U-PAM-FDM offered higher P_{avg} by 2.5 dB compared with the traditional ACO-OFDM scheme.

References

1. P. A. Hoeher, *Visible Light Communications: Theoretical and Practical Foundations*, Carl Hanser Verlag GmbH Co KG, Munich, Germany (2019).
2. Z. Ghassemlooy et al., *Visible Light Communications: Theory and Applications*, CRC Press, Boca Raton, Florida (2017).
3. T. Fath and H. Haas, "Performance comparison of MIMO techniques for optical wireless communications in indoor environments," *IEEE Trans. Commun.* **61**(2), 733–742 (2013).
4. Y. Hong, T. Wu, and L. Chen, "On the performance of adaptive MIMO-OFDM indoor visible light communications," *IEEE Photonics Technol. Lett.* **28**(8) 907–910 (2016).
5. O. Narmanlioglu et al., "Link adaptation for MIMO OFDM visible light communication systems," *IEEE Access* **5**, 26006–26014 (2017).
6. S.-W. Wang et al., "A high-performance blue filter for a white-LED-based visible light communication system," *IEEE Wireless Commun.* **22**(2), 61–67 (2015).
7. N. Fujimoto and S. Yamamoto, "The fastest visible light transmissions of 662 Mb/s by a blue LED, 600 Mb/s by a red LED, and 520 Mb/s by a green LED based on simple OOK-NRZ modulation of a commercially available RGB-type white LED using pre-emphasis and post-equalizing techniques," in *Eur. Conf. Opt. Commun.*, IEEE, Cannes, France, pp. 1–3 (2014).

8. X. Huang et al., "1.6 Gbit/s phosphorescent white LED based VLC transmission using a cascaded pre-equalization circuit and a differential outputs PIN receiver," *Opt. Express* **23**(17), 22034–22042 (2015).
9. H. Li et al., "A 550 Mbit/s real-time visible light communication system based on phosphorescent white light LED for practical high-speed low-complexity application," *Opt. Express* **22**(22), 27203–27213 (2014).
10. P. A. Haigh et al., "Visible light communications: 170 Mb/s using an artificial neural network equalizer in a low bandwidth white light configuration," *J. Lightwave Technol.* **32**(9), 1807–1813 (2014).
11. X. Li et al., "Should analogue pre-equalisers be avoided in VLC systems?" *IEEE Photonics J.* **12** (2), 7901014 (2020).
12. H. Marshoud et al., "Optical non-orthogonal multiple access for visible light communication," *IEEE Wireless Commun.* **25**(2), 82–88 (2018).
13. C. Chen et al., "On the performance of MIMO-NOMA-based visible light communication systems," *IEEE Photonics Technol. Lett.* **30**(4), 307–310 (2018).
14. M. Wolf and M. Haardt, "On the DC balance of multi-level PAM VLC systems," in *21st Int. Conf. Transp. Opt. Networks*, IEEE, Angers, France, pp. 1–5 (2019).
15. R. Bian, I. Tavakkolnia, and H. Haas, "15.73 Gb/s visible light communication with off-the-shelf LEDs," *J. Lightwave Technol.* **37**(10), 2418–2424 (2019).
16. J. Armstrong and A. J. Lowery, "Power efficient optical OFDM," *Electron. Lett.* **42**(6), 370–372 (2006).
17. S. C. J. Lee et al., "PAM-DMT for intensity-modulated and direct-detection optical communication systems," *IEEE Photonics Technol. Lett.* **21**(23), 1749–1751 (2009).
18. O. Saied, et al, "Position encoded asymmetrically clipped optical orthogonal frequency division multiplexing in visible light communications," *J. Commun. Inf. Networks* **2**(4), 1–10 (2017).
19. M. P. S. Bhadoria, G. Pandey, and A. Dixit, "Performance evaluation of visible light communication for DCO and ACO optical OFDM techniques," in *Natl. Conf. Commun.*, IEEE, Bangalore, India, pp. 1–6 (2019).
20. O. Saied et al., "Pilot-aided asymmetrically clipped optical OFDM in visible light communication," *Mediterr. J. Electron. Commun.* **12**(2), 64–71 (2016).
21. T. Q. Wang, H. Li, and X. Huang, "Analysis and mitigation of clipping noise in layered ACO-OFDM based visible light communication systems," *IEEE Trans. Commun.* **67**(1), 564–577 (2019).
22. W. Hu, "PAPR reduction in DCO-OFDM visible light communication systems using optimized odd and even sequences combination," *IEEE Photonics J.* **11** (1), 1–15 (2019).
23. R. Mesleh, "OFDM and SCFDE performance comparison for indoor optical wireless communication systems," in *19th Int. Conf. Telecommun.*, IEEE, Jounieh, Lebanon, pp. 1–5 (2012).
24. K. Acolatse, Y. Bar-Ness, and S. K. Wilson, "Novel techniques of single-carrier frequency-domain equalization for optical wireless communications," *EURASIP J. Adv. Signal Process.* **2011**, 393768 (2011).
25. C. Wu, H. Zhang, and W. Xu, "On visible light communication using LED array with DFT-spread OFDM," in *IEEE Int. Conf. Commun.*, IEEE, Sydney, Australia, pp. 3325–3330 (2014).
26. J. Zyren and W. McCoy, "Overview of the 3GPP long term evolution physical layer," Freescale Semiconductor, Inc., white paper 7, pp. 2–22 (2007).
27. H. G. Myung, L. Junsung, and D. Goodman, "Peak-to-average power ratio of single carrier FDMA signals with pulse shaping," in *17th Int. Symp. Personal, Indoor and Mob. Radio Commun.*, IEEE, Helsinki, Finland, pp. 1–5 (2006).
28. O. Saied et al., "Single carrier optical FDM in visible light communication," in *10th Int. Symp. Commun. Syst., Networks and Digital Signal Process.*, IEEE, Prague, Czech Republic, pp. 1–5 (2016).
29. O. Saied et al., "Optical single carrier-interleaved frequency division multiplexing for visible light communication systems," *Optik* **194**, 162910 (2019).

30. S. Dimitrov and H. Haas, *Principles of LED Light Communications: Towards Networked Li-Fi*, Cambridge University Press, Cambridge (2015).
31. THORLABS, "PDA36A-EC—Si switchable gain detector, 350–1100 nm, 10 MHz BW, 13 mm2, M4 taps," 2006, https://www.thorlabs.com/catalogpages/obsolete/2018/PDA36AEC.pdf.
32. T. Zhang et al., "Spectrum-efficient triple-layer hybrid optical OFDM for IM/DD-based optical wireless communications," *IEEE Access* **8**, 10352–10362 (2020).
33. J. G. Doblado et al., "Cubic metric reduction for DCO-OFDM visible light communication systems," *J. Lightwave Technol.* **33**(10), 1971–1978 (2015).
34. N. Taşpınar and M. Yıldırım, "A novel parallel artificial bee colony algorithm and its PAPR reduction performance using SLM scheme in OFDM and MIMO-OFDM systems," *IEEE Commun. Lett.* **19**(10), 1830–1833 (2015).
35. X. Liu et al., "Demonstration of bandwidth-efficient mobile fronthaul enabling seamless aggregation of 36 E-UTRA-like wireless signals in a single 1.1-GHz wavelength channel," in *Opt. Fiber Commun. Conf. and Exhib.*, IEEE, Los Angeles, pp. 1–3 (2015).
36. H. Li et al., "Improving performance of mobile fronthaul architecture employing high order delta-sigma modulator with PAM-4 format," *Opt. Express* **25** (1), 1–9 (2017).

Osama Saied received his higher diploma (Hons.) degree in electronic engineering from the High Institute for Poly Technics, Gharyan, Libya, in 2000. He worked as a networking engineer in Biruni Remote Sensing Center Tripoli, Libya, from 2001 to 2008. He received his MSc degree in communication and signal processing from the University of Newcastle upon Tyne, United Kingdom, in 2010. He received his PhD in visible light communications from Northumbria University, Newcastle upon Tyne, United Kingdom, in 2018. He has published four journal papers and one conference paper. His research interests include optical wireless communications, free-space optics, visible light communications, and RF over optics.

Zabih Ghassemlooy received his BSc (Hons.) degree in electrical and electronics engineering from Manchester Metropolitan University, United Kingdom, in 1981, and his MSc and PhD degrees from the University of Manchester, United Kingdom, in 1984 and 1987, respectively. He is currently pursuing his CEng degree. From 1987 to 1988, he was a postdoctoral research fellow with the City, University of London, United Kingdom. In 1988, he joined Sheffield Hallam University as a lecturer, where he became a professor in 1997. In 2004, he joined the University of Northumbria, Newcastle upon Tyne, as the associate dean (AD) of research with the School of Engineering. From 2012 to 2014, he was the AD of the Research and Innovation, Faculty of Engineering and Environment, where he is currently the head of the Optical Communications Research Group. He has published over 850 articles (330 journals and eight books). His research interests include optical wireless communications, free-space optics, visible light communications, radio over fiber-free space optics, and sensor networks with project funding from EU, United Kingdom Research Council and Industry.

Stanislav Zvanovec received his MSc and PhD degrees from Czech Technical University in Prague in 2002 and 2006, respectively, where he is a full professor, the deputy head of the Department of Electromagnetic Field, and a leader of the Wireless and Fiber Optics Team. He has authored two books and more than 250 journal articles and conference papers. His current research interests include free space optics and fiber optical systems, VLC, and rf over optics.

Refik Caglar Kizilirmak received his BSc and MSc degrees in electrical and electronics engineering from Bilkent University, Ankara, Turkey, in 2004 and 2006, respectively, and his PhD from Keio University, Yokohama, Japan, in 2010. He worked for the Communications and Spectrum Management Research Center, Turkey, on several telecommunication and defense industry projects. He contributed to the technical requirements document of 802.15.7r1 standardization, which will enable VLC. He has three patent applications in the field of wireless communications in US and Japan patent offices. Currently, he is with the Department of Electrical and Electronics Engineering, Nazarbayev University, Astana,

Kazakhstan. He is the recipient of the IEEE Vehicular Technology Society Japan 2008 Young Researcher's and Institute of Electronics, Information and Communication Engineers Wideband Systems Best Paper Awards.

Bangjiang Lin received his BSc and the PhD degrees from the Electronics Engineering Department, Peking University, Beijing, China, in 2010 and 2015, respectively. He joined Quanzhou Institute of Equipment Manufacturing, Haixi Institutes, Chinese Academy of Sciences, in 2015, as a lecturer, where he became an associate professor in 2017. He has published more than 100 articles of which half are science citation index indexed. His current research interests include passive optical networks and visible light communications.